AIChE

# Hydrodynamics of Cocurrent Two-Phase Flows in Slanted Porous Media—Modulation of Pulse Flow via Bed Obliquity

**Markus Schubert, Mohsen Hamidipour, Carl Duchesne, and Faïçal Larachi**
Dept. of Chemical Engineering, Laval University, Québec City, QC G1V 0A6, Canada

*DOI 10.1002/aic.12237*
*Published online June 1, 2010 in Wiley Online Library (wileyonlinelibrary.com).*

*A packed bed operated with descending gas–liquid cocurrent flows in slanted configuration to force trickle flow pattern to segregate due to gravity was studied, in addition to dependences to inclination angle of liquid saturation and pressure drop. Inception of pulse flow regime could take place regardless of inclination angle and the transition from segregated/trickle regime to pulse flow regime was experimentally determined. The Grosser et al. flow regime transition model was modified by considering only axial components of the gas and liquid superficial velocities to predict the slant-dependent shifts in transition from segregated/trickle to pulse flow and was found to agree with experimental data. Pulse flow regime at different inclinations was characterized with respect to frequency, velocity, and shape of pulses. Bed obliquity was unveiled as a new artifice to pulse flow modulation with possible prospects for catalytic reactions requiring antagonistically high-interaction regime mass transfer coefficients and partial catalyst wetting.* © 2010 American Institute of Chemical Engineers *AIChE J*, 56: 3189–3205, 2010
*Keywords: packed-bed hydrodynamics, inclination, segregation, electrical capacitance tomography, flow regime transition, transition model*

## Introduction

It is already more than 2 decades that the concept of unsteady-state operation of trickle-bed reactors is being extensively investigated. In its common assertion, trickle bed reactors operate with gas and liquid flowing cocurrently downward through a fixed bed of catalyst particles. Liquid maldistribution, poor mass transfer performances, and the risk for hot spot formation are recurrent problems in the design of trickle-flow reactors.[1] Silencing the hot spots and mitigating maldistribution through operation in pulse flow regime can be achieved though at the expense of shortened residence time of reactants. Flow modulation in trickle beds was proposed as an alternative that combines versatility in the control of residence time, improved mass transfer rates and fluids distribution, and avoidance of hot spots. In liquid-flow modulation, a constant-flux gas is often fed with prespecified binarized liquid stream. The first patented application of liquid-flow modulation could be credited to Gupta[2] where liquid pulses were meant to wet or rewet the surface of catalyst to prevent dry spots and catalyst under-utilization thereof due to partial wetting. Flow modulation was afterward explored more systematically by many researchers in a quest of further improvements. For example, ON–OFF liquid-flow modulation proved its worth concerning gas-limited reactions: depriving liquid irrigation during the OFF periods to enhance accessibility of the catalyst surface to gas-phase reactant for boosting reaction yield followed by resumption of liquid irrigation to allow removal of heat and of reaction

Correspondence concerning this article should be addressed to and Faïçal Larachi at Faical.Larachi@gch.ulaval.ca.
Current Address of M. Schubert: Forschungszentrum Dresden-Rossendorf, P.O. Box 51 05 19, 01314 Dresden, Germany.

products.[3–7] Yet, despite the enticing call of flow modulation, industry remains reluctant to commercial implementation[8] most plausibly because of challenges posed by the process control infrastructure as dictated by the unending changes in flow rate policies.

In our opinion, alternative process intensification approaches with innovative reactor configuration, which do not require flow rate modulation must be researched. Such approaches need to be easily implemented while potentially bringing some advantages over the existing configurations. Conventional trickle beds operate in vertical position; with the stipulation of a good design of distributor, liquid, and gas-phases coexist over the whole bed cross section. It is speculated that tilting the reactor could induce partial segregation of gas and liquid due to the gravitational force. Liquid would accumulate preferably nearby the reactor bottommost wall area, whereas gas would preferentially occupy the reactor uppermost wall part. Minimizing the liquid-rich area and imposing pulse-flow modulation via a control of bed inclination would cause occasional passages of liquid-rich pulses over the entire bed cross section. Consequently, the liquid fraction being retained in the wider gas-rich packing area would be renewed at will (along with removal of products and reaction heat which would be beneficial for instance in the case of gas-limited catalytic reactions). The frequency of pulse passage could be specified via flow rate assignments and bed inclination adjustment. It would be also possible to tilt the bed periodically to refresh the catalyst surface and then return back to vertical position to supply liquid washing a new catalyst for heat and product removal purposes.

Although it is not the purpose of this work to examine the claimed benefits from a reaction perspective, a grasp of conceptual knowledge for such inclined flows in packed beds in terms of hydrodynamics is required, at least to check whether or not the claimed circumstances are hypothetical or tangible.

Two-phase gas–liquid flow in slant packed-bed configurations has scarcely been studied and details in the scientific literature are almost absent. Far from representing mere academic wanderings, flows through slant porous media are encountered for example in oil production industry, for example, drilling and pumping; in marine oil field processes, where several inclined wells are drilled from a single platform toward different directions. Furthermore, considering the local geology of rock formations, nonvertical flows of natural gas and crude oil can emerge in geological rock formations by virtue of the permeability patterns in inclined fractures.

Numerous studies were reported dealing with air–water two-phase flows in inclined pipes and tubes.[9–13] Issues associated with gas–liquid and steam–water flows in inclined ducts and channels which are in particular encountered in cooling circuits of pressurized water reactors in nuclear power plants have also been investigated by several researchers.[14,15]

In contrast, inclined multiphase reactor configurations with fixed or slurry catalyst phase are rather on the fringes of three-phase hydrodynamic studies and are reported very sparsely in the literature. There are a few theoretical or experimental studies available which deal with the effect of inclination angle of the reactor. From a pragmatic standpoint, column inclination may have detrimental or beneficial effects on the performance of the reactor depending on its projected utilization. Inclined three-phase and gas–liquid fluidized beds were the objects of studies on flow regimes and their fluidization heterogeneity along with their corresponding heat and mass transfer characteristics.[16–20]

Nonvertical packed beds were only addressed in the case of horizontal position.[21–23] Abdobal et al.[22] applied a generalized single-phase Forchheimer equation to predict liquid hold-up and pressure drop. Johnston and Pollitt[21] and Abdobal et al.[22] identified three possible flow regimes that are stratified flow, dispersed bubble flow, and annular flow depending on the fluid throughputs. Iliuta et al.[24] proposed a one-dimensional two-fluid momentum based model and predicted two-phase pressure drop and external liquid hold up in horizontally positioned packed beds, which was tested on the experimental data of Abdobal et al.[22] by defining appropriate drag closure expressions for the different flow regimes prevailing in horizontal geometries.

While studying liquid maldistribution by means of a computer-generated two-dimensional trickle bed packed with uniform spheres, Zimmerman and Ng[25] considered the inclined configuration just for model predictions and validation. However, any comprehensive parametric studies analyzing the effect of inclination in packed beds for two-phase flows is so far fully disregarded.

It can be anticipated that inclination would considerably affect the flow patterns of gas–liquid cocurrent descending flows in packed-bed reactors and consequently segregated flow may appear in the bed. Thus, first of all, knowledge of the basic hydrodynamics for such inclined packed-bed configuration is compulsory where reactor parameters such as pressure drop and liquid saturation, flow regime transitions and their prediction, and pulse flow characteristics, must be elucidated.

## Experimental Setup and Operating Conditions

Figure 1 illustrates the experimental setup built to study the effect of inclination angle on the two-phase flow hydrodynamics in a slanted packed bed (6). The experiments were performed with air and kerosene (in liquid-recycle mode (1)) at room temperature and atmospheric pressure. To allow precise angular assignments, the packing-containing Plexiglas vessel ($d_r$ = 57 mm I.D.) was positioned on a special pivotable rack. The angular precision was 0.5°. The experiments were conducted over a wide range of gas and liquid superficial velocities to cover trickle flow, segregated/trickle flow and pulse flow regimes. The column was packed up to a height of 160 cm with spherical glass beads, 3 mm in diameter, resulting in a bed porosity of 0.395. The fluid properties, operating ranges, and packing and reactor specifications are summarized in Table 1. The packed bed was preventively operated in pulse flow mode to achieve full bed prewetting. To prevent the bed edges from shifting in the slanted positions, the packing was firmly immobilized between the gas–liquid distributor (3) atop and a retaining screen in the bottom. The liquid distributor consisted of 13 capillaries, each 1 mm in diameter, inserted 20-mm deep in the packing to minimize initial maldistribution of the liquid. Biased pressure measurements through uncontrollable intrusion of liquid in the connecting lines between the reactor walls and the differential pressure transmitter (7) were avoided by connecting the discharge area below the retaining screen and the gas

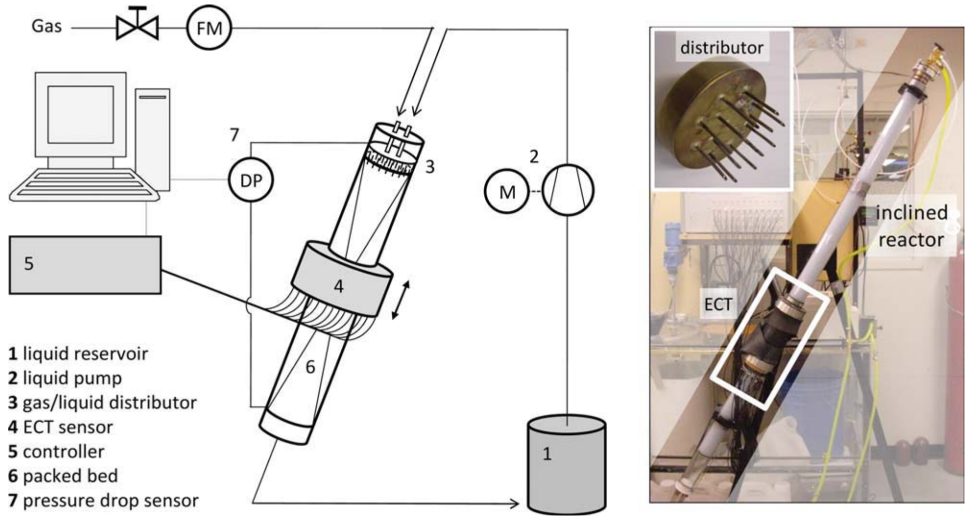


**Figure 1. Experimental setup and inclined reactor arrangement.**

[Color figure can be viewed in the online issue, which is available at wileyonlinelibrary.com.]

load section just before the distributor section (3). Bed pressure drops were thus measured with dry sampling lines though at the expense of inclusion of a little extra pressure drop by the distributor.

A 12/12-electrode twin-plane electrical capacitance tomography (ECT) sensor (PTL300E with DAM200E sensor controller, Process Tomography) with axial sliding capability was used for quantifying the liquid saturation and for substantiating the qualitative gas–liquid flow dynamics. ECT is especially suitable for imaging electrically nonconducting organic liquids such as liquid hydrocarbons of interest for our research group. The ECT scanner was mounted on a sleeve and could slide over the reactor outer diameter for interrogation of any axial region of the vessel. Owing to the twin-plane configuration, tomographic images were acquired simultaneously at two axial positions by the 2 × 12 active electrodes at a sampling rate of 50 tomographic scans per second. The two rows of measurement electrodes (50 mm high) were bounded immediately above and below with 38-mm high guard electrodes whose role was to funnel the electric field nearby the active electrodes. For each plane, 66 sets of independent capacitance measurements between electrode pairs were obtained. The measured capacitances were used to reconstruct mixture permittivity distribution out of which perpixel phase saturations were extracted (32 × 32 pixels per image). Tibirna et al.[26] implemented a finite element method to solve the Poisson equation and developed a simulator for the dispersion of the electric field inside a system characterized by nonhomogeneous permittivity distribution. Simulations were performed to compare the capability of different reconstruction algorithms to capture qualitative (shape) and quantitative (size) image features of phantoms, of predefined geometry and permittivity, inserted in cylindrical enclosures. The Tikhonov algorithm was among the most successful reconstruction approaches. Moreover, application of ECT along with this reconstruction algorithm to determine liquid saturations in trickle-bed reactors was recently validated by Hamidipour et al.[27] The same procedure was therefore used in this study to generate normalized permittivity maps from the measured capacitance data.

## Results and Discussion

### *ECT calibration*

To obtain phase volume fraction from tomographic images, the ECT sensor was calibrated at drained prewetted bed (0% reference) and at flooded bed conditions (100% reference) whose corresponding perpixel mixture permittivities could be expressed, respectively, as:

Drained pre − wetted bed

$$\alpha^{[0]} = (1-\varepsilon)\cdot\alpha_S + \varepsilon_L^{res}\cdot\alpha_L + \left(\varepsilon-\varepsilon_L^{res}\right)\cdot\alpha_G \quad (1)$$

$$\text{Flooded bed}\quad \alpha^{[1]} = (1-\varepsilon)\cdot\alpha_S + \varepsilon\cdot\alpha_L. \quad (2)$$

In two-phase flow operation, the overall permittivity can be written as:

**Table 1. Range of Experimental Data and System Properties**

| Parameter | Value/Range |
|---|---|
| Liquid superficial velocity, $u_L$ | 0.0021–0.0136 m/s |
| Gas superficial velocity, $u_G$ | 0.0616–0.3082 m/s |
| Liquid phase density, $\rho_L$ | 792.62 kg/m$^3$ |
| Liquid viscosity, $\mu_L$ | 0.0022 kg/(m s) |
| Liquid surface tension, $\sigma_L$ | 0.0253 N/m |
| Gas density, $\rho_G$ | 1.2 kg/m$^3$ |
| Glass beads diameter, $d_p$ | 3 mm |
| sphericity factor, $\phi_S$ | 1.0 |
| Bed porosity, $\varepsilon$ | 0.395 |
| Bed length, $L$ | 1.60 m |
| Dielectric constant, $\kappa$ | |
| Air | 1.00059 |
| Kerosene | 2.2 |
| Glass bead | 3.1 |
| Plexiglas | 3.4 |
| Reactor diameter, $d_r$ | 57 mm |
| Inclination angle, $\theta$ | 1.5–50° |

$$\alpha^{[GL]} = (1-\varepsilon)\cdot\alpha_S + \left(\varepsilon_L^{res} + \varepsilon_L^{fd}\right)\cdot\alpha_L + \left(\varepsilon - \varepsilon_L^{res} - \varepsilon_L^{fd}\right)\cdot\alpha_G, \quad (3)$$

where $\varepsilon$, $\varepsilon_L^{res}$ and $\varepsilon_L^{fd}$ represent, respectively, the bed porosity, the residual liquid holdup retained postdrainage in the bed due to capillary forces, and the free-draining liquid holdup; whereas, $\alpha_S$, $\alpha_L$, $\alpha_G$, are, respectively, the packing, liquid, and gas electrical permittivities. Therefore, the normalized permittivity, formed as [(3) − (1)]/[(2) − (1)], gives rise to the free-draining liquid holdup normalized by the effective void space after resting the residual liquid holdup:

$$\text{Normalized Permittivity} = \frac{\alpha^{[GL]} - \alpha^{[0]}}{\alpha^{[1]} - \alpha^{[0]}} = \frac{\varepsilon_L^{fd}}{\varepsilon - \varepsilon_L^{res}} = \beta_L^{fd}, \quad (4)$$

$\beta_L^{fd}$ is thus called the free-draining liquid saturation. All the 32 × 32 pixels of the ECT image will provide instantaneous local free-draining saturation values, $\beta_{L,i}^{fd}$, from which the cross-sectionally averaged free draining liquid saturation, $\beta_L^{fd}$, could be calculated (Eq. 5).

$$\beta_L^{fd} = \frac{1}{NP}\sum_{i=1}^{NP}\beta_{L,i}^{fd} \quad \text{and} \quad \overline{\beta_L^{fd}} = \frac{1}{NF}\sum_{j=1}^{NF}\left(\frac{1}{NP}\sum_{i=1}^{NP}\beta_{L,i}^{fd}\right). \quad (5)$$

Time-averaged liquid saturation values, $\overline{\beta_L^{fd}}$, were obtained for steady-state flow conditions from ~300 successive cross-sectional images. In this case NP and NF denote, respectively, the number of pixels and of applied frames.

Subsequently, cross-sectional averaged free-draining liquid holdup, $\varepsilon_L^{fd}$, could be calculated from Eq. 4, provided bed porosity and residual liquid holdup values are also available.

In anticipation of formation of segregated flows in inclined bed experiments, phantom measurements were performed to test the ability of the reconstruction algorithm. A closed-bottom kerosene-filled smaller diameter Plexiglas test tube (18 mm I.D.) was inserted in the bed test section close to the wall (Figures 2a1, b1). The aim was to keep liquid inside the test tube, while draining the external surrounding bed to examine the reconstructed features (shape, size) nearby the phantom area. Outside the test tube, ECT reconstruction would restore the (Eq. 1) drained prewetted bed reference point.

Two experiments were performed with the test tube. In the first, the test tube was filled with kerosene only (Figure 2a1) whereby reconstruction would restore permittivity of pure liquid (Eq. 2, $\varepsilon = 1$). In the second test, the tube was packed with 3-mm glass beads and the resulting porous space was filled with kerosene (Figure 2b1). In this latter case, the (Eq. 2) flooded bed reference point would be restored. This test was considered as the representative of inclined two-phase flows, where gas–liquid segregation taken place in the bed to allow demarcating the flooded bottom-most area (Eq. 2) in contrast to the liquid-depleted upper-most area (Eq. 1). In both phantom experiments, the lower reference points for the area inside the tube were obtained without kerosene, no matter if it were filled with glass beads (Figure 2b1) or not (Figure 2a1). Liquid in the enclosure was identified in both instances, in addition to being quantified correctly in terms of saturations by the reconstruction algorithm. Quite satisfactory results were obtained regarding the shape and size of the liquid-containing areas (Figures 2a2, b2). Although the packed test tube held lesser kerosene volume, it was still detectable and very distinguishable via ECT measurements (Figure 2b2). The computed smooth transitions in permittivity nearby the Plexiglas wall boundaries are artifactual because of the poor spatial resolution of ECT technique. It can be stated that ECT would be able to detect flow segregation in inclined two-phase flows.

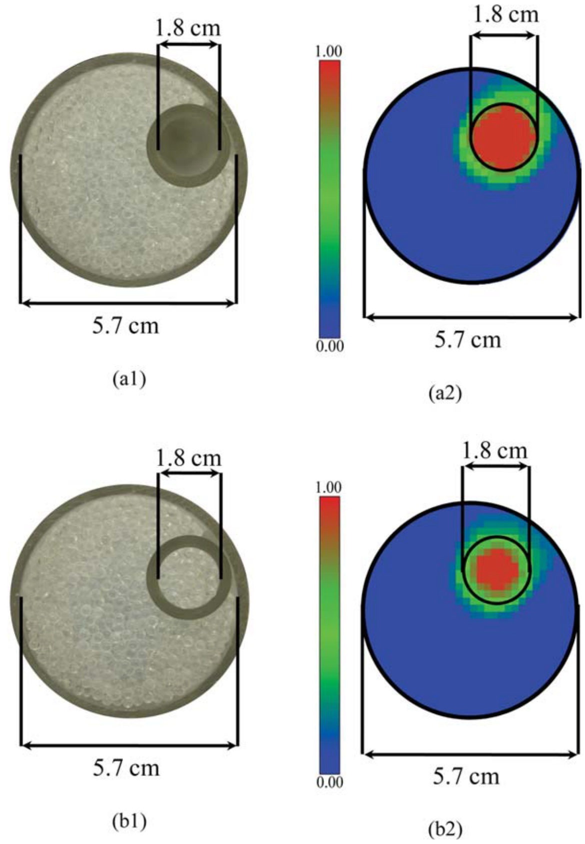


**Figure 2. Segregated flow phantoms and corresponding ECT measurements.**

[Color figure can be viewed in the online issue, which is available at wileyonlinelibrary.com.]

### *Hydrodynamic characterization of gas–liquid segregation*

As first test and departing from verticality, the drainage dynamics of bed from resting flooded state was examined as a function of increasing inclination angles (10° ≤ θ ≤ 50°). The bed was filled with kerosene, and then the exit was opened apace and completely. The instantaneous variation of liquid saturation was monitored through ECT measurements 30 cm before bed exit (Figure 3). A two-step drainage dynamics is noticeable. In the early few moments, lower inclination yields faster initial drainage by virtue of the larger stream-wise projection of gravitational acceleration, $g\cdot\cos\theta$; which is tantamount to more slanted beds retaining larger amounts of liquid. This step is subsequently followed by a distinctly slower drainage step involving the remainder of the liquid. However, a reversal in trend regarding the angular dependence of the drainage kinetics can be observed. A larger inclination angle indeed induces faster secondary

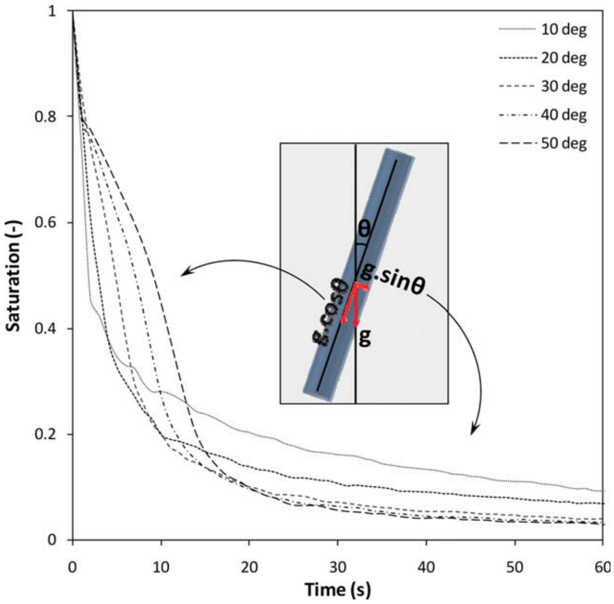


**Figure 3. Drainage of flooded bed as function of inclination degree (30 cm before bed exit).**

[Color figure can be viewed in the online issue, which is available at wileyonlinelibrary.com.]

drainage by virtue of the normal component of gravity, $g \cdot \sin \theta$, whose tendency is to pull the liquid down toward the bottom alongside the vessel wall hence minimizing liquid-packing interactions. Consequently, the liquid–solid drag force is significantly diminished, which is, conversely, tantamount to more slanted beds retaining lesser amounts of liquid.

Systematic experimental comparisons between vertically aligned trickle-bed reactors and slanted beds in two-phase flow operation were carried out to determine at which inclination angle reactor deviations in flow patterns start to occur. Therefore, the conventional straight reactor operated at different gas and liquid superficial velocities in a stable trickle flow regime was gradually inclined. The flow patterns were objectified with ECT and pressure drop measurements. Figure 4 shows the development of the free-draining liquid saturation (henceforth referred to as liquid saturation in short) over the cross section of the packed bed 70 cm downstream in the bed for inclinations varying from $\theta = 0°$ (vertical) up to 20°.

Vessel inclination obviously affects the gas–liquid distribution and flow patterns in slanted packed beds. The flow patterns evolve only slightly for low slants. At 6°, the inclination results already in a clear segregation, which becomes more pronounced at higher inclinations. The segregation state can be assessed based on the lack of crosswise uniformity of the liquid saturation distribution. A uniformity factor, $\chi$, was hence defined on the basis of deviations of perpixel saturations with respect to the cross-sectional liquid saturation obtained from Eq. 5:

$$\chi = \frac{1}{\mathrm{NF}} \sum_{i=j}^{\mathrm{NF}} \left( \frac{1}{\mathrm{NP}} \sum_{i=1}^{\mathrm{NP}} \left( \frac{\beta_{\mathrm{L},i}^{\mathrm{fd}} - \beta_{\mathrm{L}}^{\mathrm{fd}}}{\beta_{\mathrm{L}}^{\mathrm{fd}}} \right)^2 \right), \tag{6}$$

where NP denotes the number of pixels in the image, $\beta_{\mathrm{L},i}^{\mathrm{fd}}$ and $\beta_{\mathrm{L}}^{\mathrm{fd}}$ are the local liquid saturation and the average cross-sectional liquid saturation for every image, respectively. Approximately 300 successive cross-sectional images (NF) were applied to reduce bias in the estimation of the uniformity factor.

Tantamount to pronounced segregation in our context, increasing values of the uniformity factor mean aggravation of maldistribution with increased slant (Figures 4 and 5). Maldistribution starts at inclination angles larger than 6° which implies the beginning of gas–liquid segregation (Figure 5). Lower the gas superficial velocities occasion, higher the values of uniformity factor (i.e., worsening of two-phase distribution). The effect of liquid superficial velocity was marginal, except for the lowest gas superficial velocity where maldistribution seemed to invigorate from inclination angles $\theta > 6°$ due to more accumulation of liquid nearby the bottommost wall with higher liquid-flow rates.

Although the transition region from trickling flow to a developing segregated flow can be detected from Figures 4 and 5, clear segregation is expected at higher inclinations. Thus, the segregated flow study was extended to high inclination angles up to 50° and characterized regarding the effect of fluid throughputs and inclination on bed pressure drop and longitudinal development of liquid saturation starting with uniform (initial) liquid distribution.

For a detailed hydrodynamic characterization, the obtained cross-sectional liquid saturation data were analyzed with respect to the average liquid saturation (Eq. 5) and to the pressure drop (Figures 6a, b) at a 70 cm position downstream in the bed.

The liquid saturation (Figure 6a) is clearly affected by the inclination angle for all superficial fluid velocities as investigated in this study. Already at very small deviations from straight vertical position, the average liquid saturation started

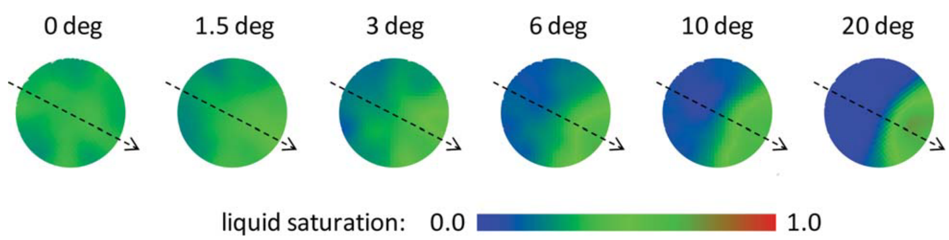


**Figure 4. Exemplary illustration of the inclination effect on the flow texture ($u_L$ = 0.0021 m/s, $u_G$ = 0.0616 m/s, 70 cm downstream in the bed).**

[Color figure can be viewed in the online issue, which is available at wileyonlinelibrary.com.]

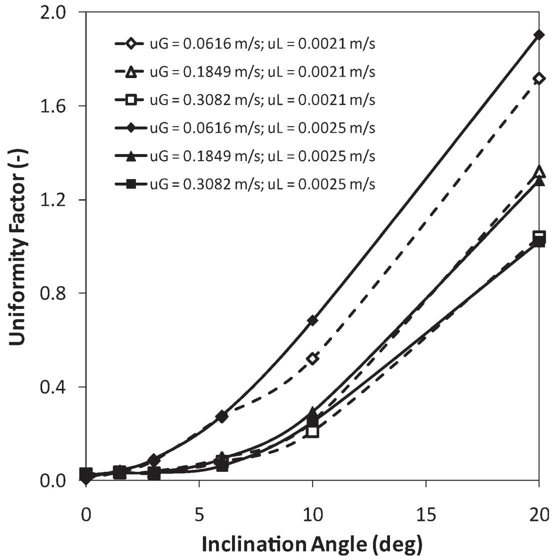


**Figure 5. Effect of inclination angle on uniformity criterion (70 cm downstream in the bed).**

to drop down. Higher gas flow rates resulted in lower liquid saturations in agreement with literature findings for beds in upright positions.[28,29] Increasing gas superficial velocity results in increased shear stress at the gas–liquid interface, so liquid saturation accordingly decreases. The effect of gas superficial velocity on the magnitude of liquid saturation is more pronounced at low inclination angles because of better gas–liquid distribution over the cross section and thus higher interactions between the gas and liquid phases. At inclination angles higher than 10°, clear segregation has already developed (see Figure 4) thereby reducing the level of interactions between the fluid phases. The effect of inclination at higher angles decreases clearly and the liquid saturations tend to plateau at values determined by the gas and liquid superficial velocities (Figure 6a).

Analysis of the pressure drop data (Figure 6b) confirms lower fluid interactions due to segregation by a decreasing trend at inclination angles $\theta > 10°$. At conditions with clearly developed segregation, the pressure drop decreases with higher inclinations as the ratio of the bed cross section covered by the liquid phase shrinks. However, contrary to the clear decreasing trend of the liquid saturation already at low inclinations ($\theta < 10°$) the pressure drop is almost not affected in the same range of inclination angles. Furthermore, at low superficial gas velocity the effect of inclination angle was nearly negligible regardless of inclination. In line with literature observations,[28,29] pressure drop increases with increasing gas and liquid superficial velocities due to more pronounced gas–liquid and fluid–solid interactions; though with a more pronounced effect of superficial gas velocity in the investigated range.

During segregation, liquid saturation was measured via ECT at different heights along the reactor (Figure 7). Measurement spots were in particular carried out in the region close to the bed entrance. However, because of geometrical restrictions of the experimental setup (ECT sensor unit length), the first scans could be performed only starting from a distance of 14.5 cm after bed entrance. Figure 7 shows that the axial development, until a translation-invariant segregation state is attained, is clearly affected by fluid velocities and inclination angle. Higher liquid and gas superficial velocities require longer entrance distances before the cross-sectionally average liquid saturations stabilize in the streamwise direction (Figure 7a, c). Higher inclinations on the contrary force two-phase flow segregations to develop over shorter distances after the bed entrance (Figure 7b). The tiny plateau near the top of the bed at an inclination angle of 10°

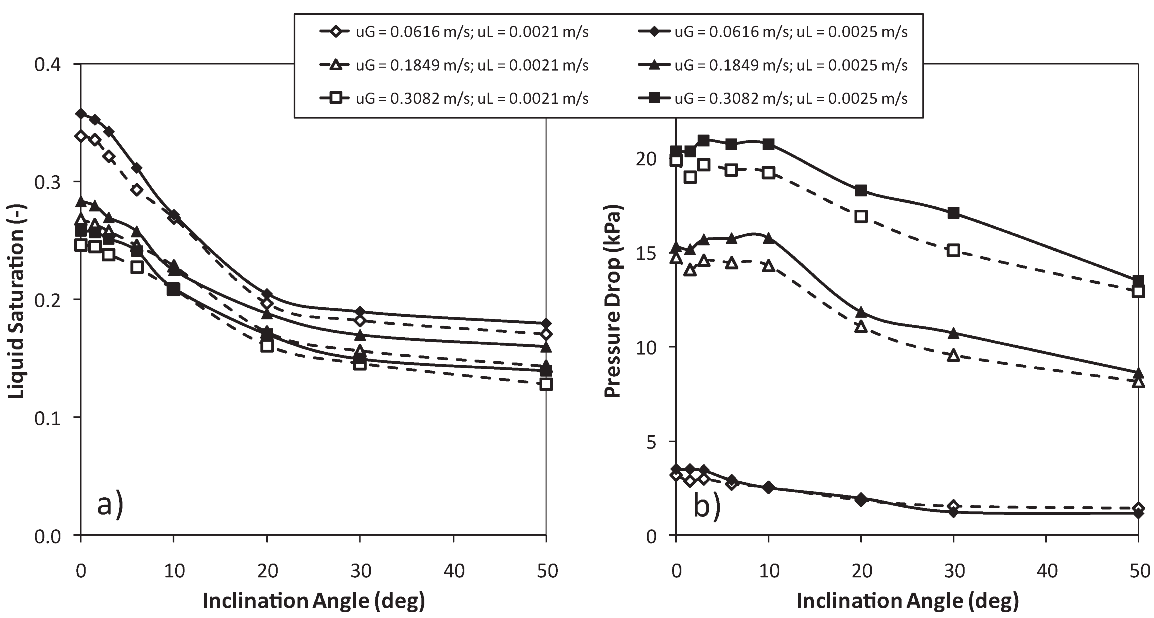


**Figure 6. Effect of inclination angle (a) on cross-sectional average liquid saturation (70 cm downstream in the bed) and (b) on pressure drop.**

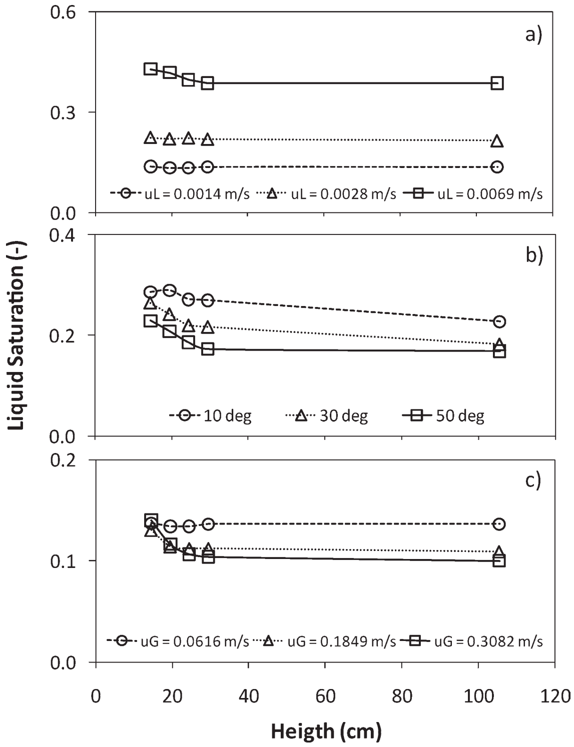


**Figure 7. Effect of superficial fluid velocities and inclination angle on axial liquid saturation profiles, (a) 50°, $u_G = 0.0616$ m/s, (b) $u_G = 0.0616$ m/s, $u_L = 0.0028$ m/s, and (c) 50°, $u_L = 0.0014$ m/s.**

indicates that segregation initiated at superficial fluid velocities of $u_G = 0.0616$ m/s and $u_L = 0.0028$ m/s is not yet remarkable.

The hydrodynamic data demonstrate clearly that inclined packed-bed reactors behave differently in low interaction regimes from the well-known vertical trickle flow mode because inclination results in gas–liquid segregation in the bed. Pulse flow regime could be a method to operate inclined reactors using the whole bed cross section in a periodic manner. Therefore, it has to be shown, if pulse flow can be achieved in slanted geometries and how the pulse flow characteristics could be affected by increased inclination angle.

### *Onset of pulse flow regime*

It is obvious that conventional flow regime maps of trickle beds (e.g., proposed by Charpentier and Favier[30] and Gianetto and Specchia[31]) are inadequate for the determination of the onset of pulsing flow in slanted beds since the transition to pulse flow might also occur from a distinctively new flow pattern, that is, segregated/trickle flow regime as observed for high inclinations, which does not exist in vertical flows. However, setting a new regime transition map applicable for slanted two-phase flows in porous media will require identifying regime changeover as a function of inclination angle, bed axial location where flow transition is being scrutinized, and preferably, along with the underlying mechanisms. Visual observation revealed that the onset of pulsing for given gas flow rate and axial location occurred at different liquid superficial velocities which were dependent on inclination angles. Thus, the transition from trickle flow (for low inclinations) or segregated/trickle flow (for higher inclinations) to pulse flow was observed visually for selected axial positions 30 cm away from top or from bottom of the packing.

Figure 8a shows the transition to natural pulsing flow regime for different inclination angles, 30 cm away from the reactor bottom. Between 0° and 7.5° the effect of low inclination angles on the transition (highlighted in grey and bounded by dashed lines) was marginal with a tendency to no effect at all toward increased gas flow rates. Higher inclinations, on the contrary, resulted in important extensions of

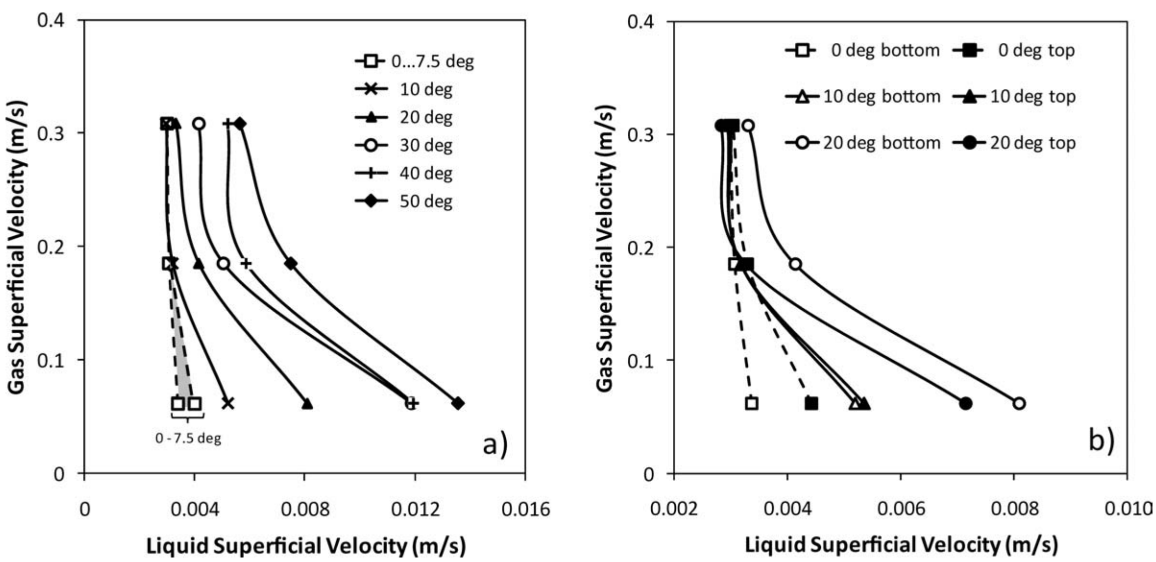


**Figure 8. (a) Onset of natural pulsing as a function of the inclination angle 30 cm away from reactor bottom and (b) transition mechanism changeover (top = 30 cm away from reactor top, bottom = 30 cm away from reactor bottom).**

the segregated/trickle flow toward the higher liquid velocities.

To get insight into the mechanism of regime changeover, the regime transitions determined at the top and bottom sections of the reactor were compared for inclination angles of 0°, 10°, and 20°. (Figure 8b). It was shown experimentally that the transition to pulse flow for slightly inclined reactors ($\theta < 10°$) follows known instability inception. The onset of pulses occurred first nearby the exit of the reactor and propagated upward with increasing fluid throughputs similar to the phenomenon for trickle beds, for example, as shown by Boelhouwer et al.[32] However, at an inclination angle of 10°, the onset of pulsing was observed at the same velocities both at the bottom and top parts of the reactor. Tilting toward steeper inclination angles ($\theta > 10°$) revealed that pulsing was initiated by liquid waves in the upper reactor part propagating downward and requiring increased liquid superficial velocity for the changeover to occur in the bottom part. The initial pulsing in upper part can be characterized as a wavy pulse flow expanding over the whole cross section that achieves fully developed pulse flow by accumulating increasing amounts of liquid downstream. It can be concluded that application of conventional models analyzing the loss of stability of steady-state trickle flow features[33] has to be considered with caution.

However, to characterize the flow patterns that evolve at the transition from segregated/trickle flow to pulsing regime, noninvasive ECT can be applied as well. Each ECT image represents a two-dimensional tomogram averaged over 5 cm high slices in the reactor corresponding to the electrodes' height. An Eulerian slice representation of ECT images is used to visualize the axial development of the liquid-flow field.[34] Pixelized liquid saturations (Eq. 4) reconstructed along a selected diametrical line (e.g., A-A line in Figure 9a) are shot in a volley at 50 Hz pace as recorded and plotted one after the other from individual images recorded during two-phase flow operation. In the current instance, the perpendicular line A-A crossing the segregated liquid area from bottommost to uppermost wall areas at a given axial position is the most representative line. Evolving this line time-wise from bottom to top as in Figure 9a, would be tantamount to pick up "upstream" events for the flow direction but delayed in time until they hit the tomograph sensing plane. This gives, in an approximate sense, virtually local axial tomogram representation of the liquid-flow field. Figures 9b, c are typical images used to build the Eulerian slices ($\theta = 40°$). Each row shows different instants of a pulse passage under specific operating conditions recorded 30 cm above the bottom of the reactor. The first row (Figure 9b) was obtained at the transition from segregated/trickle to pulse flow ($u_G = 0.154$ m/s and $u_L = 0.009$ m/s). The second row (Figure 9c) presents different moments of persistent pulse flow ($u_G = 0.308$ m/s and $u_L = 0.009$ m/s) established by increasing gas superficial velocity for the same liquid superficial velocity. Several images (17 sec × 50 Hz) similar to these two rows were used to construct Figures 9d–f (i.e., Eulerian slices). Under trickle flow regime ($u_G = 0.062$ m/s and $u_L = 0.0023$ m/s) and vertically positioned bed ($\theta = 0$), slightly lower liquid saturations are observed close to the walls which is attributed to the higher porosity in this region (Figure 9d). Furthermore, the Eulerian slices in trickle flow regime confirm persistence, and thus stability with time, of this regime. Tilting the bed by $\theta = 40°$ (Figure 9e) forces the liquid to migrate toward the bottom section (or lower wall) and to trickle in a segregated manner; however, the liquid saturation values close to the bottommost wall indicate still the presence of gas phase. It should be noted that the extent of segregation and phase holdup over the cross section depends on the flow rates and inclination degree. Increasing gas and liquid superficial velocities will enhance the interaction between gas and liquid and can initiate pulses as shown in Figure 9f for an inclination of $\theta = 40°$ and for gas and liquid superficial velocities of 0.154 m/s and 0.009 m/s, respectively.

Considering the other way around, that is, fading out of the pulsing flow, for constant gas and liquid velocities ($u_L = 0.0048$ m/s, $u_G = 0.062$ m/s) Figure 10 illustrates the change in distribution morphology and flow regime as function of inclination angle. Under the selected operating conditions, vertical bed ($\theta = 0°$) operates in pulse flow regime (Figure 10a). Tilting gradually the bed favors segregation, therefore pulses turn into new forms of instabilities as shown in Figure 10b ($\theta = 10°$). Further increased inclinations can result in complete segregation. The interaction between phases diminishes significantly and the pulses totally disappear. As discussed earlier, accumulation of liquid phase nearby the bottommost wall depends on the inclination degree and superficial velocities. Figure 10d ($\theta = 50°$) reveals higher volume fraction of liquid close to the bottommost wall when compared to Figure 10c ($\theta = 30°$). As the velocities are constant in this case, more liquid accumulation is attributed to inclination angle. Even closer to this lower wall, liquid saturations exhibit lower values because of higher bed porosity in this area (Figure 10c, $\theta = 30°$).

These experiments reveal a new possibility of controlling the periodicity of pulses, via bed obliquity, in pulse flow regime. In vertical position, beds experience pulse flows ensuring high mass transfer rates with no possible modulation of catalyst wetting efficiency as complete wetting is permanently maintained in such flow regime. This can be undesirable, especially when gas-limited catalytic reactions are of interest and for which conversion can be lowered by the liquid-film mass transfer resistance no matter how much this can be attenuated. Inclined configuration, on the contrary, suggests controllable liquid resistance and wetting efficiency, therefore potentially providing a much flexible accessibility of gas to catalyst surface.

### *Pulse flow characteristics*

To study the morphology of two-phase flow under pulse flow regime, the Eulerian slices were plotted for the early pulses forming in the transition region from segregated/trickle to pulse and for the fully developed pulse flow regime (Figures 11a–c). Liquid superficial velocity was kept constant ($u_L = 0.009$ m/s) whilst gas superficial velocity was increased stepwise ($u_G = 0.154$, 0.231, 0.308 m/s) for an inclination angle $\theta = 40°$. Close to the bottommost wall the liquid accumulation displays a wavy pattern with pulses occasionally forming at the transition between segregated/trickle and pulse flow regimes (Figure 11a). These pulses are strong enough to burst and sweep the whole cross section at

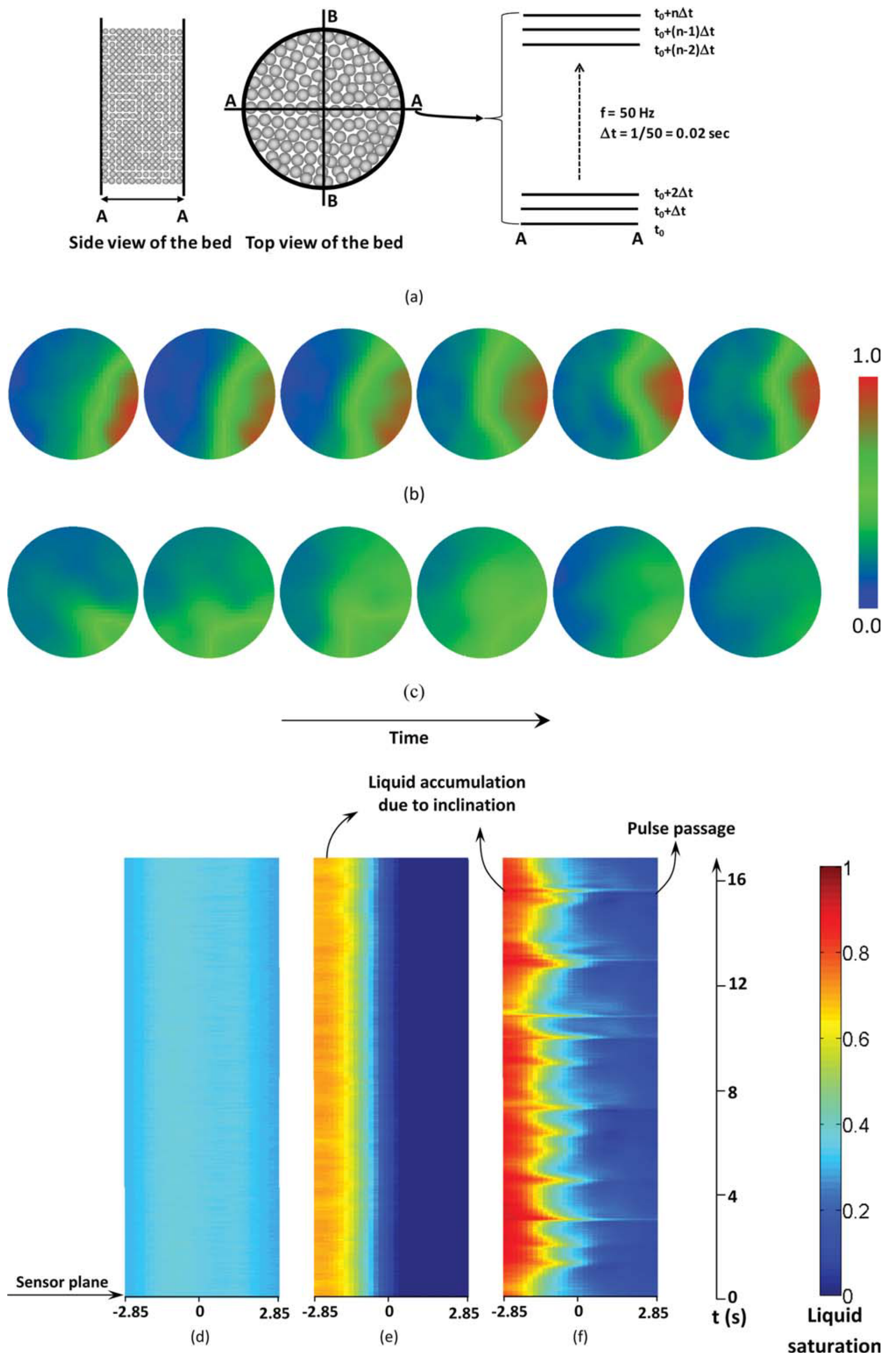


**Figure 9. ECT images, (a) Schematic of Eulerian slice construction, (b) ECT snapshots of segregated-trickle to pulse flow regime transition, $u_G$ = 0.154 m/s, $u_L$ = 0.009 m/s, $\theta$ = 40°, (c) ECT snapshots of developed pulse flow in inclined bed, $u_G$ = 0.308 m/s, $u_L$ = 0.009 m/s, $\theta$ = 40°, (d) axial liquid field under trickle flow in vertical bed, $u_G$ = 0.062 m/s, $u_L$ = 0.002 m/s, $\theta$ = 0°, (e) axial liquid field under segregated-trickle flow in inclined bed, $u_G$ = 0.062 m/s, $u_L$ = 0.002 m/s, $\theta$ = 40°, and (f) axial liquid field under transition from segregated-trickle to pulse flow regime in inclined bed, $u_G$ = 0.154 m/s, $u_L$ = 0.009 m/s, $\theta$ = 40°.**

[Color figure can be viewed in the online issue, which is available at wileyonlinelibrary.com.]

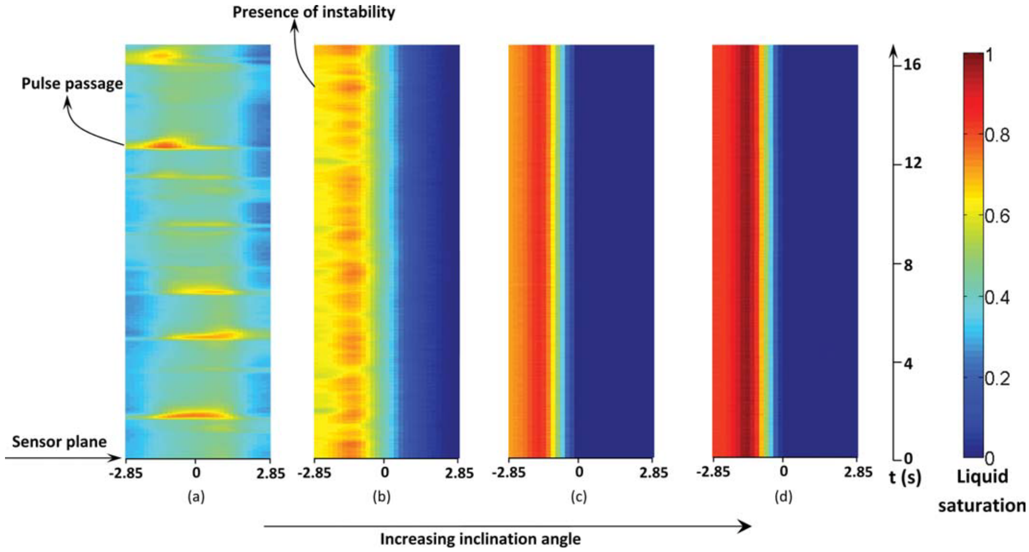


**Figure 10. ECT Eulerian slices as function of inclination angle, fade out of pulsation ($u_L$ = 0.005 m/s, $u_G$ = 0.062 m/s), (a) θ = 0°, (b) θ = 10°, (c) θ = 30°, and (d) θ = 50°.**

[Color figure can be viewed in the online issue, which is available at wileyonlinelibrary.com.]

a given axial location. Accumulation of liquid nearby the bottommost wall decreases by increasing gas superficial velocity (Figure 11b) at the expense of a persistent pulse flow regime. Further increased superficial gas velocity (Figure 11c) results in sharp and strong pulses able to momentarily remove lower-wall liquid accumulation.

To compare the structure of pulses with the conventional configuration (θ = 0°), axial Eulerian slices of the bed under the same operating conditions ($u_L$ = 0.009 m/s, $u_G$ = 0.154, 0.231, 0.308 m/s) are illustrated in Figures 11d–f. Figure 11d shows that under the superficial velocities corresponding to transition for inclined bed (Figure 11a), the vertical reactor is already in developed pulse flow regime because of the higher interaction between gas and liquid. The liquid slugs are thick and cover almost the entire cross section; however, for most liquid slugs, higher liquid saturations prevail preferentially in the core region. Although consisting of two-phase mixtures, liquid slugs are liquid richer at lower gas velocities. Augmenting gas superficial velocity reduces both size and liquid content of the slugs (Figure 11e). Figure 11f illustrates that further increase of gas superficial velocity can produce more uniform and thin pulses. In general, under the same conditions, increasing gas superficial velocity tends to reduce the morphological contrasts between the inclined and vertical positions.

The behaviors of pressure drop signals are compared in vertical (θ = 0°) and inclined (θ = 40°) beds (Figures 12a, b, respectively) for the same gas and liquid velocities ($u_L$ = 0.009 m/s, $u_G$ = 0.154, 0.231, 0.308 m/s). Unlike with ECT, not all pulses can be resolved separately in the pressure drop signals as bed pressure measurements are global, merge, and/or confound the several pulses coexisting at the same time along the reactor. Figure 12b shows that at the lowest gas velocity, the inclined bed experiences lesser pressure drop due to the fact that most often the phases flow in a segregated manner. Whenever gas–liquid interactions give rise to pulses, pressure drop rises to levels matched by those in the vertical bed configuration. For higher gas velocities pressure, drop signals are qualitatively similar regardless of inclination thus making features extraction and analysis from pressure time series even more ambiguous.

Although the Eulerian slices focused on the spatial shape of the pulses, more basic temporal characteristics of the pulsing flow regime such as the pulse velocity and pulse frequency[35] can also be extracted from an analysis of ECT images. Figure 13 shows exemplarily time series of the (cross-sectionally averaged) pulsing liquid saturation for inclination angles of 0° and 50°. Recall that liquid saturations are measured simultaneously at two axial positions with the two sensor planes. Note that the 50° saturations were purposely plotted not at scale to highlight the difference in the qualitative features vis-à-vis the 0° configuration. It can be seen that over the same time duration, the number and temporal shape of pulses strongly depend on bed inclination.

For different gas and liquid velocities, which resulted in persistent pulse flow conditions at all inclination angles up to 50°, pulse velocity and pulse frequency were derived by applying, respectively, spatial cross-correlation analysis and perplane fast Fourier transforms to the time-series of liquid saturation for both electrode planes of the ECT sensor. The pulse velocity was computed from the time lag maximizing the cross-correlation between the delayed liquid saturation time series obtained at the two sensor levels knowing the distance between sensor planes. The dominant pulse frequency was extracted from the estimated averaged power spectral densities of the liquid saturation data assembled into >40 packets of 2048 data points each.[27] For all conditions, pulse flow history was recorded by ECT for 30 min at 50 Hz for straight and inclined configurations alike. Time series of liquid saturation which contained more than 2000 pulses were analyzed. In Figure 14, the results for pulse velocity and pulse frequency are shown, respectively, as a function of bed inclinations. For vertical reactor, the level of gas and liquid-flow rates in the investigated range had no effect on

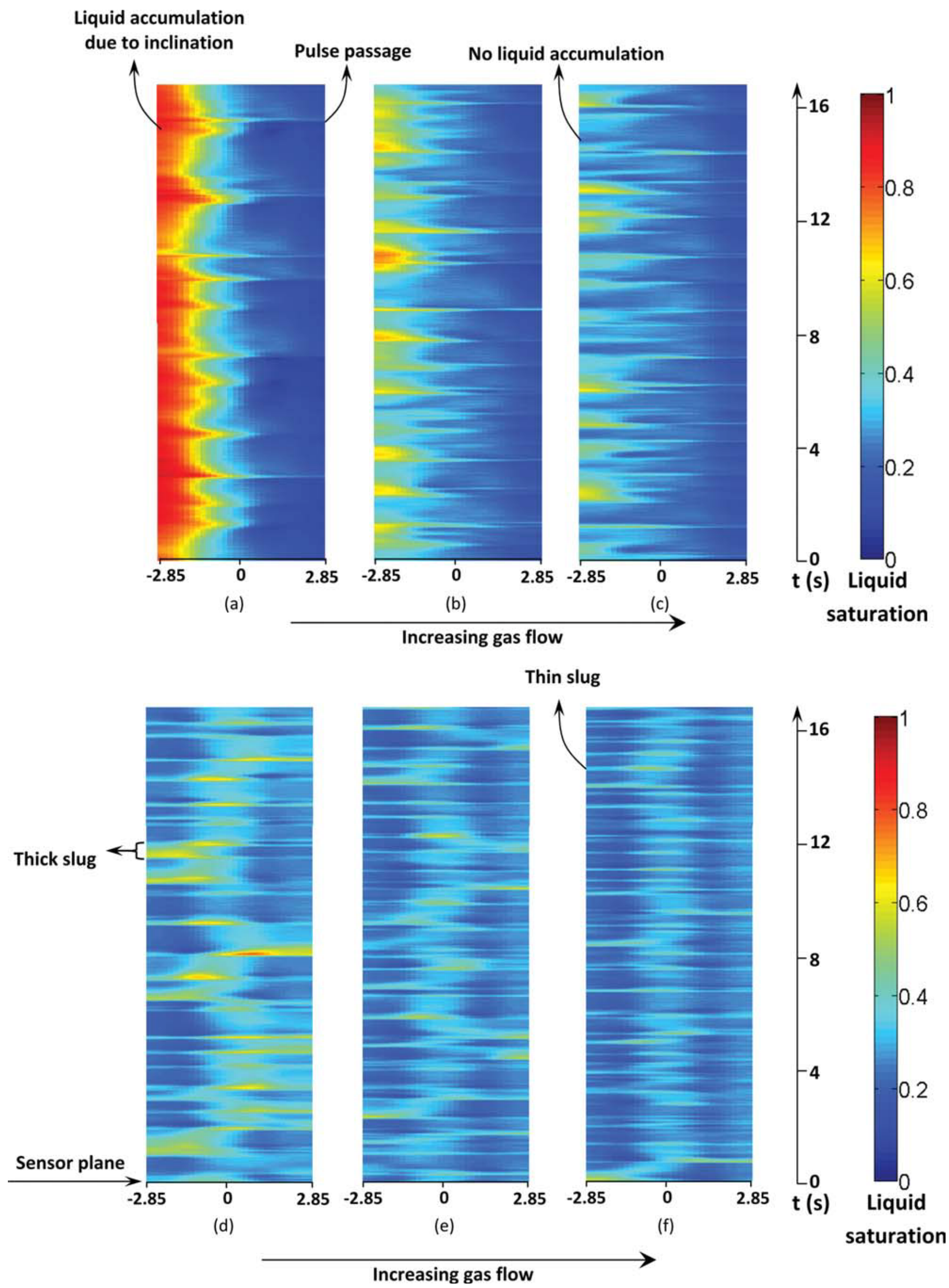


**Figure 11. ECT axial plots of pulse flow in inclined bed at θ = 40° (a–c) and vertical bed at θ = 0° (d–f), $u_L$ = 0.009 m/s, (a, d) $u_G$ = 0.154 m/s, (b, e) $u_G$ = 0.231 m/s, (c, f) $u_G$ = 0.308 m/s.**

[Color figure can be viewed in the online issue, which is available at wileyonlinelibrary.com.]

the level of pulse velocity in accordance with literature findings.[35,36] For inclined configurations, only at low superficial gas velocities ($u_G$ = 0.154 m/s) that pulse velocity was affected by inclination angle following a threshold process. There exists a critical angle below which pulse velocity was indifferent to inclination and above which pulse velocity decreased with increasing inclination angle. This threshold inclination angle increased with increasing liquid velocity. It can be concluded that the pulse shape for fully developed pulsing and thus the gas/liquid pulse interactions are constant, suggesting that the effect of gravity in the pulse flow mode is marginal for inclinations smaller than the threshold angle.

The pulse frequency shows a decreasing behavior with increasing inclination angle regardless of fluid superficial velocities investigated. No threshold inclination angle was observed for pulse frequency. Therefore, to transport the same amount of liquid at lower pulse frequency, longer pulses or pulses with distinctive tails would be expected as will be analyzed next.

Apart from pulse velocity and pulse frequency, the temporal pulse shape seems to be drastically affected by bed

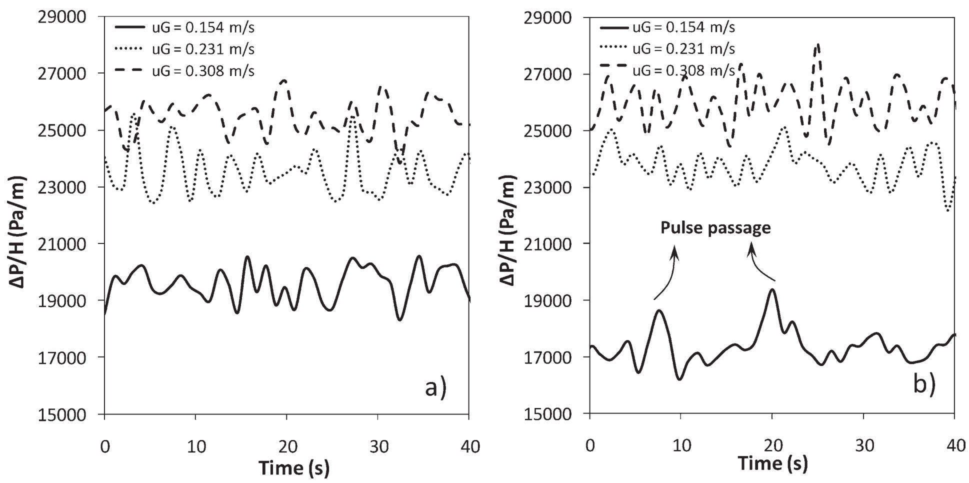


**Figure 12. Time evolution of overall pressure drop signals, $u_L$ = 0.009 m/s, $u_G$ = 0.154, 0.231, 0.308 m/s, (a) vertical bed (θ = 0°) and (b) inclined bed (θ = 40°).**

inclination. Thus, the pulse maxima-to-minima height ratio, $\Delta H_{\mathrm{P,i}}$, was analyzed (Eq. 7, for definition see Figure 13). Furthermore, the slope of the pulses after the peak maxima was fitted with an exponential expression, $f(\lambda_{\mathrm{P,i}})$, (Eq. 8, for definition see Figure 13). $\beta_{\mathrm{L},0}$ represents the asymptotic liquid saturation.

$$\Delta H_{\mathrm{P,i}} = \frac{\beta^{\mathrm{fd}}_{\mathrm{L,max,Pi}_i}}{\beta^{\mathrm{fd}}_{\mathrm{L,min,Pi}_i}} = \beta^{\mathrm{fd}}_{\mathrm{L,max,Pi}_i} \cdot \frac{1}{\min\left|\beta^{\mathrm{fd}}_{\mathrm{L}}\right|^{t_{\mathrm{P}_i}}_{t_{\mathrm{P}_{i+1}}}}, \tag{7}$$

$$\beta^{\mathrm{fd}}_{\mathrm{L,P}_i}(t - t_{\mathrm{P}_i}) = \left(\beta^{\mathrm{fd}}_{\mathrm{L,max,P}_i} - \beta^{\mathrm{fd}}_{\mathrm{L},0}\right) \cdot \exp\left(-\lambda_{\mathrm{P},i} \cdot (t - t_{\mathrm{P}_i})\right) + \beta^{\mathrm{fd}}_{\mathrm{L},0}, \quad t \geq t_{\mathrm{P}_i}. \tag{8}$$

Statistical pulse shape analysis was performed for gas and liquid velocities of 0.154 and 0.009 m/s, respectively, for the straight reactor configuration and inclined reactors up to 50° applying Eqs. 7 and 8. These experimental conditions represent the case with the most pronounced effect of inclination angle in the range investigated (see Figure 14). Normalized distributions of the characteristic data, $\Delta H_{\mathrm{P,i}}$ and $\lambda_{\mathrm{P,i}}$ were calculated from more than 2000 pulses (Figure 15).

The mode of the normalized pulse maxima-to-minima height ratio distribution (Figure 15a) is not affected by the inclination angle until 30°. ($\Delta H_{\mathrm{P}} \approx 1.35$). The distribution is nearly symmetric and the spreading of the ratio distribution is also stable. Only for high inclination angles (40° and 50°), the distribution mode shifts toward lower ratios. This is in agreement with the expectations derived from pulse frequency and pulse velocity analysis. The slowly decreasing liquid saturation after a pulse peak at high inclination angles does not reach comparatively low minima before the next pulse has initiated increasing values. This characteristic tailing becomes more obvious by considering the distribution of $\lambda_{\mathrm{P}}$. For inclination angles up to 20°, the distribution mode is nearly constant ($\lambda_{\mathrm{P}} \approx 13$). With higher inclination angles the mode strongly tends toward lower values of $\lambda_{\mathrm{P}}$; the distribution is clearly right skewed and becomes narrower. Here, lower values for $\lambda_{\mathrm{P}}$ indicate pronounced tailing after the pulse peak and thus the same amount of liquid is transported in spite of lower pulse frequency, as alluded to above.

## Modeling of Flow Regime Transition Between Segregated/Trickle Flow and Pulse Flow

Numerous models for prediction of flow regime transition from trickle to pulse flow in packed beds were published. One approach relates the bed scale pulsing to pore scale phenomena (i.e., occlusion of packing channels) applying critical hydrodynamic parameters for liquid holdup and pressure drop at the onset of pulsing,[37–39] whereas other more general approaches view the inception of pulsing as a loss of stability of the trickle flow regime which is proposed with macroscopic scale models.[33,40] Grosser et al.[33] have predicted the transition by considering a one-dimensional hydrodynamic model for the trickling regime based on the volume-averaged conservation equations for volume, mass (incompressible version) and momentum (Eqs. 9–11):

$$\varepsilon_{\mathrm{L}} + \varepsilon_{\mathrm{G}} = \varepsilon \tag{9}$$

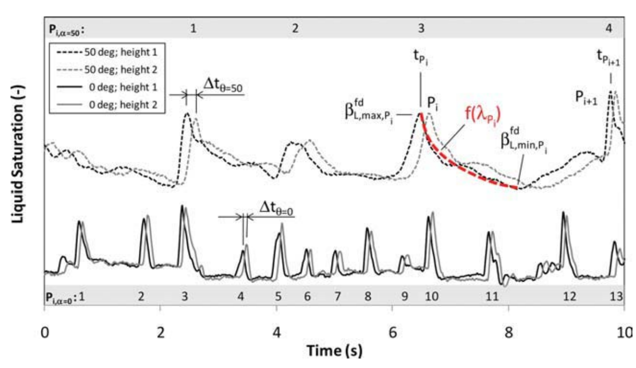


**Figure 13. Effect of inclination on pulse characteristics at two ECT heights ($u_G$ = 0.1541 m/s, $u_L$ = 0.0090 m/s).**

[Color figure can be viewed in the online issue, which is available at wileyonlinelibrary.com.]

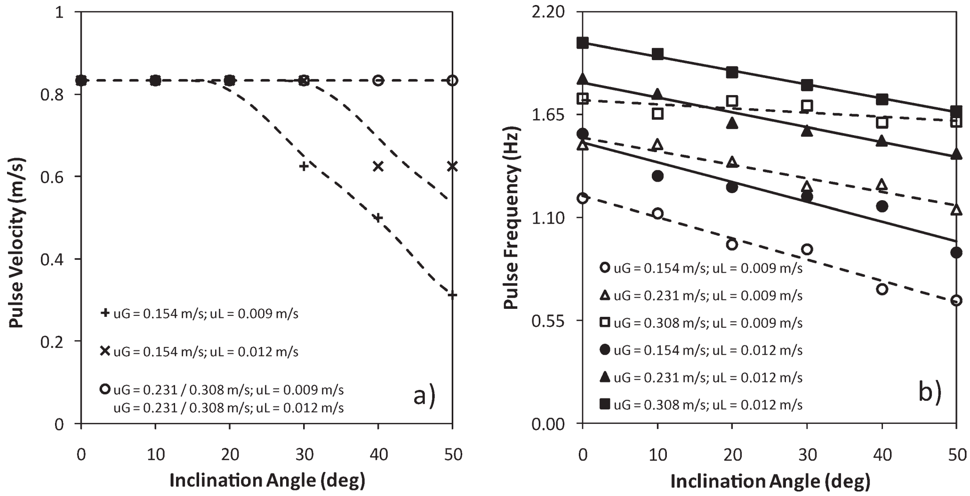


**Figure 14. Global pulse flow characteristics at different inclination angles (a) pulse velocity and (b) pulse frequency.**

$$\frac{\partial \varepsilon_i}{\partial t} + \nabla \cdot (\varepsilon_i \cdot u_i) = 0 \qquad i = \mathrm{G, L} \tag{10}$$

$$\rho_\mathrm{i} \cdot \varepsilon_\mathrm{i} \cdot \left\{ \frac{\partial u_i}{\partial t} + u_i \cdot \nabla u_i \right\} = -\varepsilon_i \nabla p_i + \varepsilon_i \cdot \rho_i \cdot g + F_i + \nabla \cdot [\varepsilon_i \cdot \tau_i + \varepsilon_i \cdot R_i] \quad i = \mathrm{G, L}. \tag{11}$$

The onset of pulsing was defined as a loss of stability of the steady state (indicated by superscript 0) solutions (Eqs. 12 and 13) or as a loss of the existence of any solution.

$$\varepsilon_\mathrm{L}^0 + \varepsilon_\mathrm{G}^0 = \varepsilon \tag{12}$$

$$\frac{F_\mathrm{G}^0}{\varepsilon_\mathrm{G}^0} - \frac{F_\mathrm{L}^0}{\varepsilon_\mathrm{L}^0} + (\rho_\mathrm{G} - \rho_\mathrm{L}) \cdot g = 0 \tag{13}$$

Assuming one-dimensional perturbations around this uniform state, a stability criterion was derived that defines the trickling-to-pulsing transition (Eq. 14).

$$W_1 \cdot W_5^2 + 2 \cdot W_1 \cdot W_3 \cdot W_5 + W_2^2 \cdot W_4 = 0, \tag{14}$$

with

$$W_1 = \sum_i \frac{\rho_i}{\varepsilon_i^0}, W_2 = -\sum_i \frac{\alpha_i}{\left(\varepsilon_i^0\right)^2},$$

$$W_3 = \sum_i \frac{\rho_i \cdot u_i^*}{\varepsilon_i^0}, W_4 = \sum_i \frac{\rho_i \left(u_i^*\right)^2}{\varepsilon_i^0} + \sigma_\mathrm{L} \cdot \sqrt{\frac{\varepsilon}{k}} \cdot \frac{\partial J}{\partial \varepsilon_\mathrm{L}},$$

$$W_5 = \frac{F_\mathrm{G}^0}{\left(\varepsilon_\mathrm{G}^0\right)^2} + \frac{F_\mathrm{L}^0}{\left(\varepsilon_\mathrm{L}^0\right)^2} - \frac{\xi_\mathrm{G}}{\varepsilon_\mathrm{G}^0} - \frac{\xi_\mathrm{L}}{\varepsilon_\mathrm{L}^0} + \frac{\zeta_\mathrm{G} \cdot u_\mathrm{G}^*}{\left(\varepsilon_\mathrm{G}^0\right)^2} + \frac{\zeta_\mathrm{L} \cdot u_\mathrm{L}^*}{\left(\varepsilon_\mathrm{L}^0\right)^2},$$

$$\text{where } \zeta_i = \left(\frac{\partial F_i}{\partial u_i^*}\right)^0, \xi_i = \left(\frac{\partial F_i}{\partial \varepsilon_i}\right)^0 \text{ and } \sqrt{\frac{\varepsilon}{k}} = \frac{(1-\varepsilon)}{\varepsilon \cdot \mathrm{d_p}} \cdot \sqrt{A}, J = 0.48 + 0.036 \ \ln\left(\frac{\varepsilon - \varepsilon_\mathrm{L}}{\varepsilon_\mathrm{L}}\right).$$

The drag forces are given in Eqs. 15 and 16.

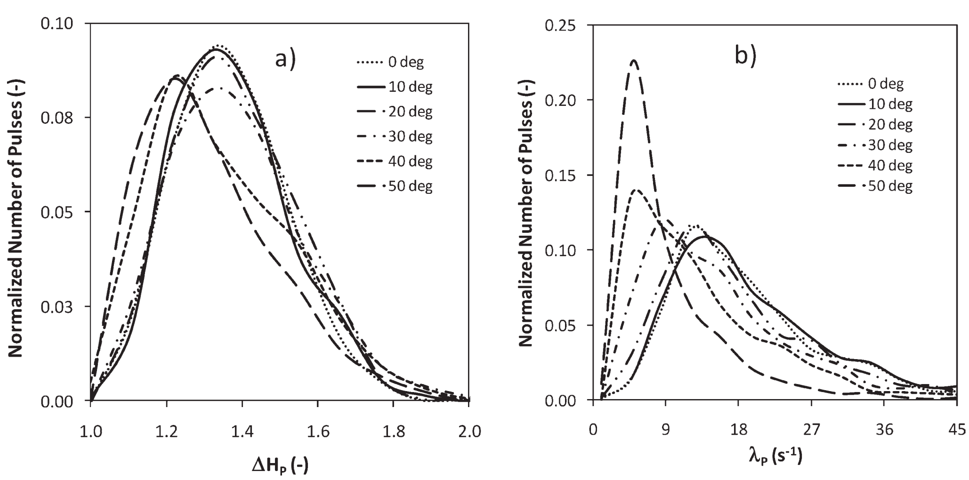


**Figure 15. Pulse shape analysis at different inclination angles (a) Pulse maxima-to-minima height ratio distribution and (b) Distribution of the peak slope exponent.**

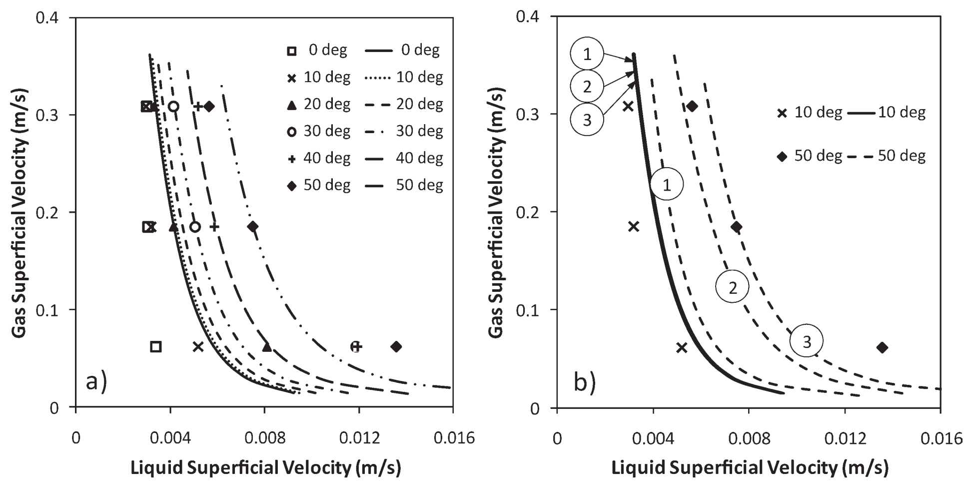


**Figure 16. (a) Flow regime transition map, experiments vs. simulation and (b) prediction depending on considered velocity components, Case 1: $u^*_G = u_G \cos\theta$, $u^*_L = u_L$, Case 2: $u^*_L = u_L \cos\theta$, $u^*_G = u_G$, and Case 3: $u^*_{L/G} = u_{L/G} \cos\theta$.**

$$F_G = -\left\{\frac{A\cdot\mu_G\cdot(1-\varepsilon)^2\cdot\varepsilon^{1.8}}{d_p^2\cdot\varepsilon_G^{2.8}} + \frac{B\cdot\rho_G\cdot(1-\varepsilon)\cdot\varepsilon^{1.8}\left|u^*_G\right|}{d_p\cdot\varepsilon_G^{1.8}}\right\}\cdot u^*_G, \tag{15}$$

$$F_L = -\left\{\frac{\varepsilon-\varepsilon_{L,st}}{\varepsilon_L-\varepsilon_{L,st}}\right\}^{2.9} \cdot\left\{\frac{A\cdot\mu_L\cdot(1-\varepsilon)^2\cdot\varepsilon_L^2}{d_p^2\cdot\varepsilon^3} + \frac{B\cdot\rho_L\cdot(1-\varepsilon)\cdot\varepsilon_L^3\left|u^*_L\right|}{d_p\cdot\varepsilon^3}\right\}\cdot u^*_L \tag{16}$$

The static liquid holdup is estimated from correlations proposed by Sáez and Carbonell[41] in Eq. 17.

$$\varepsilon_{L,st} = (20 + 0.9\cdot Eo^*)^{-1} \text{ with } Eo^* = \frac{\rho_L\cdot g\cdot d_p^2\cdot\varepsilon^2}{\sigma_L\cdot(1-\varepsilon)^2}. \tag{17}$$

No effect of reactor inclination is expected on the static-liquid holdup. Unlike Munteanu and Larachi[42] who modified the gravitational terms to consider micro/macrogravity, here we propose to include reactor inclination in the drag forces and in the definition of the stability criteria via an intuitive modification of the vertical fluid velocity components as shown in Eq. 18 to discuss the transition between the segregated/trickle flow regime and pulse flow regime for the high inclination angles:

$$u^*_i = u_i\cos\theta \tag{18}$$

This modification of net volumetric fluid fluxes is suggested through two pragmatic motivations. The first relates to the fact that for large inclinations segregated/trickle flow would have already established so that part of gas and liquid velocities will have already split between the bottommost liquid-rich and uppermost gas rich domains. Hence, Eq. 18 accounts for the lowered gas and liquid fluxes in the (lower-part) liquid-rich, wherein instabilities toward pulsing flow will necessarily have to originate. The second motivation behind using Eq. 18 is suggested by the drainage patterns discussed in Figure 3 above, where it was shown that the rapid drainage dynamics

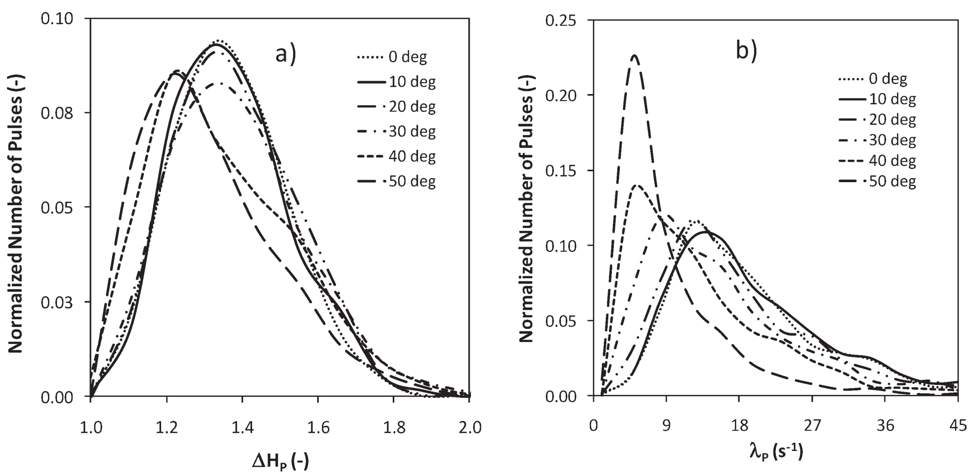


**Figure 17. Effect of (a) particle diameter ($\varepsilon$ = 0.395) and (b) packing porosity ($d_p$ =3 mm) on flow regime transition at different inclination angles.**

portion were mostly driven by gravitational effects of the net gravity component projected along the stream-wise direction.

In an attempt to back the experimental observations discussed above, the simulations of the transition from segregated/trickle to pulse flow were performed for air/kerosene system and current packing properties. The transitional velocities were determined over the range of experimentally explored gas and liquid velocities. Only the experimental flow regime transition velocities at the bottom of the reactor were compared with the simulation results to neglect any effects of entrance length at the top of the reactor. The inclination effect on the segregated/trickling-to-pulsing flow transition was estimated with the modified Grosser et al.[33] model and the results, including experimental data, are shown in Figure 16a.

First, it can be concluded that experimental and simulated data are in pretty close agreement. Deviations are obvious at lower gas flow rates, even without inclination. However, the simulated values for higher superficial gas flow rates are conclusive and imply that the model can be used as a predictive tool for inclined packed beds operating up to 50° inclinations. The model accounts for the minor effect of low inclinations (up to 20°) and drastic effects at higher inclination angles.

Additionally, the effect of considered velocity components in the drag force formulation (Eqs. 15 and 16) and in the stability criterion (Eq. 14) was investigated. Figure 16b shows the model predictions and the experimental transition data for reactor inclinations of 10° and 50°. For both inclinations angles, three different scenarios are considered: only the axial velocity component ($u^*$) of the gas (Case 1) or the liquid (Case 2) phase is modified according to Eq. 18 while superficial velocity is assumed for the other fluid phase (Case 1 and 2, respectively) and the third case where Eq. 18 is applied simultaneously to both phases in the model. At 10° inclination there is no effect on simulated transition shifts of the choice of velocity components. However, different flow regime transition simulated curves are obtained for 50° inclination. A delayed transition, in accordance with experimental observations, is predicted from the model through amending one axial velocity component at a time (Case 1 or Case 2) for 50° inclination. Wider enlargement of segregated/trickle flow regions are the resultant of liquid velocity attenuation, followed to a lesser extent, by gas velocity attenuation. Although the effect of liquid velocity is clearly more pronounced, it still under-predicts the transition shift as measured experimentally had the corresponding axial gas velocity been not considered. Applying Eq. 18 to both gas and liquid velocities (Case 3) yields very conclusive agreement between experimental observations and simulated transition.

Applying the modified Grosser et al.[33] model considering both gas and liquid axial velocity components, the regime transition was simulated for packings of 1 and 5 mm (Figure 17a) and for bed porosities of 0.330 and 0.395 (Figure 17b), while keeping each time packing porosity and particle diameter, respectively, constant.

At constant gas flow rates, lower particle diameters shift the regime transition toward higher liquid superficial velocities, particularly at higher gas flow rates which is in agreement with the literature (e.g., see excel worksheet simulator for packed beds[43]). Although lower packing porosities result in a shift toward lower liquid superficial velocities due to their stronger resistance to gas–liquid flow, the qualitative shapes of the flow regime transition lines are preserved. In both cases, the delayed transition to the pulsing flow regime is more pronounced at higher inclination angles, which is attributed to the cosine function feature between 0° and 90°.

## Conclusions

For the first time, comprehensive hydrodynamic experiments were performed for packed beds considering reactor inclinations up to 50°. Although their application in chemical engineering is yet to be found, this new configuration could indeed contribute to process intensification combining unit operations, such as chemical reaction and fluid transport while using at the same time shortened vessel lengths thanks to inclination. Furthermore, inclined packed-bed reactors could be applied as an alternative to periodic operation opening a new vision toward enhanced operation where liquid pulses with frequencies and velocities depend on inclination angle and pressure drops can be lowered compared with vertically operated periodic reactors. These experiments reveal a new possibility of controlling via bed obliquity the periodicity of pulses in pulse flow regime. In vertical position, beds experience pulse flows ensuring high mass transfer rates with no possible modulation of catalyst wetting efficiency as complete wetting is permanently maintained in pulse flow regime. This can be undesirable, especially when gas-limited catalytic reactions are of interest and for which conversion can be lowered by the liquid-film mass transfer resistance no matter how much it can be improved. Inclined configuration, on the contrary, suggests controllable liquid resistance and wetting efficiency, therefore potentially providing a much improved accessibility of gas to catalyst surface.

It is obvious that two-phase flow in porous media results in new segregated flow patterns and different hydrodynamic behavior. The hydrodynamics in slanted beds was studied with regard to pressure drop and liquid saturation, flow regime transition and its model prediction, and the pulse flow characteristics.

Segregation initiated for inclinations higher than 5° and clearly developed at inclination angles higher than 10°. The liquid saturation is strongly affected by the inclination angle. Already at very small deviations from straight vertical orientation, the average liquid saturation started to decrease. The effect of inclination angle at higher angles decreases and the values tend to plateau at levels determined by the level of gas and liquid superficial velocities. Although pressure drop is not affected by the inclination for angles lower than 10°, at higher inclinations its behavior confirms lower fluid interactions due to segregation. Furthermore, it was shown that development of flow pattern from uniform initial distribution toward equilibrium segregated flow is forced by higher inclination angles while high fluid velocities counteract the development of segregation.

The transition from segregated/trickle flow to natural pulsing flow regime occurs at higher fluid velocities. The effect becomes more pronounced at higher inclination angles. Especially inclination at low gas flow rates shifts the transition drastically toward higher liquid velocities. Although pulse flow is characterized by a decreasing frequency because of higher inclinations for all fluid velocities; pulse velocity decreases only at low superficial gas velocities starting from a certain threshold inclination angle.

A theoretical analysis based on a modified Grosser et al.[33] transition model was attempted. Only the axial (or streamwise) components of the superficial fluid velocities were taken into account ($u_i^* = u_i \cos \theta$) in the stability model whereby model predictions were in qualitative and quantitative agreement with experimental findings.

Within this study, an enhanced conceptual knowledgebase for inclined flows in packed beds is provided and recommendations for operation of such reactor configurations can be derived.

## Acknowledgments

One of the authors (M.S.) gratefully acknowledges the Government of Canada for its financial support during his postdoctoral fellowship in Laval University. Financial support from F.L. Canada Research Chair "Green processes for cleaner and sustainable energy," and authors' Discovery Grants from the Natural Sciences and Engineering Research Council (NSERC) is gratefully acknowledged.

## Notation

$A$, $B$ = Ergun constants
$d$ = diameter, m
$Eo^*$ = Eotvos number, $\rho_L g d_p^2 \varepsilon^2 (\sigma_L (1-\varepsilon)^2)^{-1}$
$F$ = drag force per unit bed volume, kg/(m$^2$s$^2$)
$g$ = acceleration due to gravity, m/s$^2$
$\Delta H$ = height ratio
$J$ = Leverett J function
$k$ = relative permeability parameter
$L$ = bed length, m
NF = number of frames
NP = number of pixels
p = pressure, Pa
R = pseudo-turbulence stress tensor, kg/(m$^2$s$^2$)
t = time, s
$u$ = superficial velocity, m/s
$u^*$ = axial component superficial velocity, m/s
$W_1 \ldots W_5$ = see Eq. 14

### Greek letters

$\alpha$ = electrical permittivity, F/m
$\beta$ = liquid saturation
$\chi$ = uniformity criterion
$\varepsilon$ = packing porosity
$\varepsilon_G$ = gas holdup
$\varepsilon_L$ = liquid holdup
$\Phi_S$ = sphericity factor
$\lambda$ = peak slope exponent, 1/s
$\mu$ = dynamic viscosity, kg/(m s)
$\rho$ = density, kg/m$^3$
$\sigma$ = surface tension, N/m
$\tau$ = viscous stress tensor, kg/(m$^2$s$^2$)
$\theta$ = inclination angle, °
$\kappa$ = dielectric constant (ratio of permittivity of substance to permittivity of vacuum)
$\xi$ = see Eq. 14
$\zeta$ = see Eq. 14

### Subscripts

G = gas phase
L = liquid phase
max = maximum
min = minimum
p = particle
P = peak
r = reactor
S = solid
st = static
0 = asymptotic

### Superscripts

0 = uniform steady state and drained state of the bed
1 = flooded state of the bed
fd = free-draining
G = gas
L = liquid
res = residual

### Abbreviation

ECT = electrical capacitance tomography

## Literature Cited

1. Boelhouwer JG, Piepers HW, Drinkenburg AAH. Advantages of forced non-steady operated trickle-bed reactors. *Chem Eng Technol*. 2002;25:647–650.
2. Gupta R. Pulsed flow vapor-liquid reactor. US Pat. 4,526,757, 1985
3. Lange R, Hanika J, Stradiotto D, Hudgins RR, Silveston PL. Investigation of periodically operated trickle-bed reactors. *Chem Eng Sci*. 1994;49:5615–5621.
4. Lange R, Schubert M, Dietrich W, Grünewald M. Unsteady-state operation of trickle-bed reactors. *Chem Eng Sci*. 2004;59:5355–5361.
5. Khadilkar M, Al-Dahhan MH, Dudukovic MP. Parametric study of unsteady-state flow modulation in trickle-bed reactors. *Chem Eng Sci*. 1999;54:2585–2595.
6. Khadilkar M, Al-Dahhan MH, Dudukovic MP. Multicomponent flow-transport-reaction modeling of trickle bed reactors: application to unsteady state liquid flow modulation. *Ind Eng Chem Res*. 2005;44:6354–6370.
7. Urseanu MI, Boelhouwer JG, Bosman HJM, Schroijen JC. Induced pulse operation of high-pressure trickle bed reactors with organic liquids: hydrodynamics and reaction study. *Chem Eng Process*. 2004;43:1411–1416.
8. Schubert M, Bauer T, Lange R. Instationäre Betriebsweise zur Leistungssteigerung technischer Rieselbettreaktoren. *Chem Ing Tech*. 2006;78:1023–1032.
9. Barnea D, Shoham O, Taitel Y. Flow pattern transition for downward inclined two phase flow; Horizontal to vertical. *Chem Eng Sci*. 1982;37:735–740.
10. Taitel Y, Dukler AE. A model for predicting flow regime transitions in horizontal and near horizontal gas-liquid flow. *AIChE J*. 1976;22:47–55.
11. Spedding PL, Watterson JK, Raghunathan SR, Ferguson MEG. Two-phase co-current flow in inclined pipe. *Int J Heat Mass Transfer*. 1998;41:4205–4228.
12. Merchuk JC, Rosenblat Y, Berzin I. Fluid flow and mass transfer in a counter-current gas-liquid inclined tubes photo-bioreactor. *Chem Eng Sci*. 2007;62:7414–7425.
13. Cheng TW, Lin TL. Characteristics of gas-liquid two-phase flow in small diameter inclined tubes. *Chem Eng Sci*. 2001;56:6393–6398.
14. Ousaka A, Deendarlianto, Kariyasaki A, Fukano T. Prediction of flooding gas velocity in gas-liquid counter-current two-phase flow in inclined pipes. *Nucl Eng Des*. 2006;236:1282–1292.
15. Vallee C, Deendarlianto, Beyer M, Lucas D, Carl H. Air/water counter-current flow experiments in a model of the hot leg of a pressurized water reactor. *J Eng Gas Turbines Power Trans ASME*. 2009;131:022905.
16. O'Dea DP, Rudolph V, Chong YO, Leung LS. The effect of inclination on fluidized beds. *Powder Technol*. 1990;63:169–178.
17. Del Pozo M, Briens CL, Wild G. Effect of column inclination on the performance of three-phase fluidized beds. *AIChE J*. 1992;38:1206–1212.
18. Hudson C, Briens CL, Prakash A. Effect of inclination on liquid-solid fluidized beds. *Powder Technol*. 1996;89:101–113.
19. Yakubov B, Tanny J, Maron DM, Brauner N. The dynamics and structure of a liquid-solid fluidized bed in inclined pipes. *Chem Eng J*. 2007;128:105–114.

20. Valverde JM, Castellanos A, Quintanilla MAS, Gilabert FA. Effect of inclination on gas-fluidized beds of fine cohesive powders. *Powder Technol*. 2008;182:398–405.
21. Johnston IW, Pollitt RR. Horizontal two-phase flow of liquid water/water vapour through packed beds. *Trans IChemE*. 1979;57:256–261.
22. Abdobal S, Fourar M, Radilla G, Moyne C, Lenormand R. Effects of high velocity on air-water two-phase flow through porous media. Presented at the 4th International Conference on Multiphase Flow, USA, 2001.
23. Fourar M, Lenormand R, Larachi F. Extending the F-function concept to two-phase flow in trickle beds. *Chem Eng Sci*. 2001;56: 5987–5994.
24. Iliuta I, Fourar M, Larachi F. Hydrodynamic model for horizontal two-phase flow through porous media. *Can J Chem Eng*. 2003;81:1–6.
25. Zimmerman SP, Ng KM. Liquid distribution in trickling flow trickle-bed reactors. *Chem Eng Sci*. 1986;41:861–866.
26. Tibirna C, Edouard D, Fortin A, Larachi F. Usability of ECT for quantitative characterization of trickle-bed flow dynamics subject to filtration conditions. *Chem Eng Process*. 2006;45:538–545.
27. Hamidipour M, Larachi F, Ring Z. Monitoring filtration in trickle beds using electrical capacitance tomography. *Ind Eng Chem Res*. 2009;48:1140–1153.
28. Larachi F, Laurent A, Midoux N, Wild G. Experimental study of a trickle bed reactor operating at high pressure: two-phase pressure drop and liquid saturation. *Chem Eng Sci*. 1991;46:1233–1246.
29. Al-Dahhan MH, Dudkovic MP. Pressure drop and liquid holdup in high pressure trickle-bed reactors. *Chem Eng Sci*. 1994;49:5681–5698.
30. Charpentier JC, Favier M. Some liquid holdup experimental data in trickle bed reactors for foaming and non-foaming hydrocarbons. *AIChE J*. 1975;21:1213–1218.
31. Gianetto A, Specchia V. Trickle-bed reactors: state of art and perspectives. *Chem Eng Sci*. 1992;47:3197–3213.
32. Boelhouwer JG, Piepers HW, Drinkenburg AAH. Nature and characteristics of pulsing flow in trickle-bed reactors. *Chem Eng Sci*. 2002;57:4865–4876.
33. Grosser K, Carbonell RG, Sundaresan S. Onset of pulsing in two-phase concurrent downflow through a packed bed. *AIChE J*. 1988;34:1850–1860.
34. Reinecke N, Mewes D. Investigation of the two-phase flow in trickle-bed reactors using capacitance tomography. *Chem Eng Sci*. 1997;52:2111–2127.
35. Blok JR, Drinkenburg AAH. Hydrodynamic properties of pulses in two-phase downflow operated packed columns. *Chem Eng J*. 1982;25:89–99.
36. Aydin B, Larachi F. Trickle bed hydrodynamics and flowregime transition at elevated temperature for a Newtonian and a non-Newtonian liquid. *Chem Eng Sci*. 2005;60:6687–6701.
37. Sicardi S, Gerhard H, Hofmann H. Flow regime transition in trickle-bed reactors. *Chem Eng J*. 1979;18:173–182.
38. Sicardi S, Hofmann H. Influence of gas velocity and packing geometry on pulsing inception in trickle bed reactors. *Chem Eng J*. 1980;20:251–253.
39. Ng KM. A model for regime transitions in concurrent down-flow trickle bed reactors. *AIChE J*. 1986;32:115–122.
40. Holub RA, Dudukovic MP, Ramachandran PA. Pressure drop, liquid holdup, and flow regime transition in trickle flow. *AIChE J*. 1993;39:302–321.
41. Sáez AE, Carbonell RG. Hydrodynamic parameters for gas-liquid concurrent flow in packed beds. *AIChE J*. 1985;31:52–62.
42. Munteanu MC, Larachi F. Flow regimes in trickle beds using magnetic emulation of micro/macrogravity. *Chem Eng Sci*. 2009;64:391–402.
43. Larachi F, Grandjean B. *Excel Worksheet Simulator for Packed Beds*. The Chemical Engineering Department, Laval University: Quebec City, 1999. Available at: http://www.gch.ulaval.ca/grandjean/pbrsimul/pbrsimul.html. Accessed September 23, 2009.

*Manuscript received Oct. 6, 2009, and revision received Feb. 16, 2010.*